

Thermo-mechanical damage of tungsten surfaces exposed to rapid transient plasma heat loads

Tamer Crosby and Nasr M. Ghoniem*

**Department of Mechanical & Aerospace Engineering, University of California at Los Angeles (UCLA),
420 Westwood Plaza, Los Angeles, CA 90095-1597, USA*

(Received December 13, 2010, Accepted April 14, 2011)

Abstract. International efforts have focused recently on the development of tungsten surfaces that can intercept energetic ionized and neutral atoms, and heat fluxes in the divertor region of magnetic fusion confinement devices. The combination of transient heating and local swelling due to implanted helium and hydrogen atoms has been experimentally shown to lead to severe surface and sub-surface damage. We present here a computational model to determine the relationship between the thermo-mechanical loading conditions, and the onset of damage and failure of tungsten surfaces. The model is based on thermo-elasticity, coupled with a grain boundary damage mode that includes contact cohesive elements for grain boundary sliding and fracture. This mechanics model is also coupled with a transient heat conduction model for temperature distributions following rapid thermal pulses. Results of the computational model are compared to experiments on tungsten bombarded with energetic helium and deuterium particle fluxes.

Keywords: tungsten; Plasma-Facing Components (PFC); helium ions; cracks; grain boundary damage; swelling.

1. Introduction

In nuclear fusion reactors, Plasma-Facing Components (PFC), such as the divertor, are subjected to high fluxes of energetic photons, neutrons, and hydrogen and helium ions. The impingement of these energetic atom fluxes leads to rapid and transient heating of the surface. Bombardment by helium isotopes leads to helium-induced damage accompanying micro-structural evolution, such as material swelling and the formation of blisters (Xu *et al.* 2007), dislocation loops, and helium holes or bubbles (Iwakiri *et al.* 2000). Several recent experiments (see references Tokunaga 2003, Tokunaga *et al.* 2002) have shown that the damage in the surface region and inside the material may degrade the thermophysical properties as well as the optical reflectivity of tungsten.

Divertors in fusion reactors are subjected to transient plasma events characterized with high thermal energy for short durations. One class of these transient events is the Edge-Localized Mode (ELM), which is a highly nonlinear magnetohydrodynamic event that is accompanied by periodic expulsion of particles and high thermal energy (3-10% of the core thermal energy). Typical values for ELM energies are 0.1-0.5 MJ/m² for the Joint European Torus (JET) and 1-5 MJ/m² for the

* Corresponding author, Professor, E-mail: ghoniem@ucla.edu

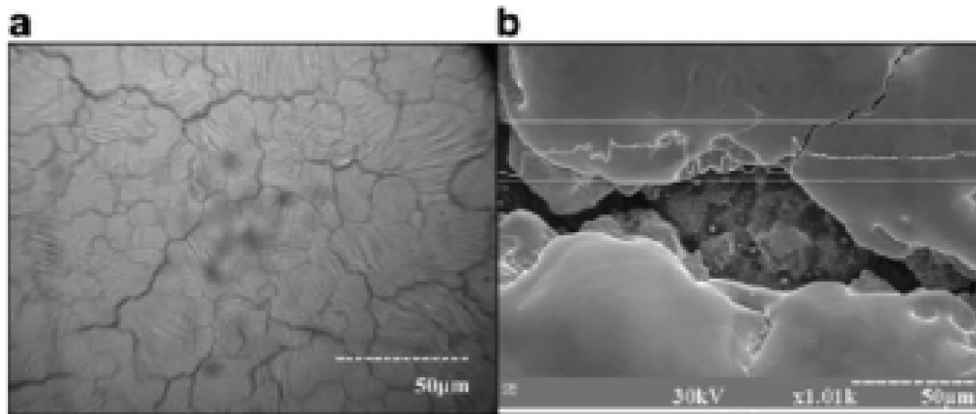


Fig. 1 Cracks on the tungsten surface after 80 and 310 plasma pulses of 0.75 MJ/m^2 (Garkusha *et al.* 2009)

International Thermonuclear Experimental Reactor (ITER). The duration of ELM events are relatively short, 0.1-1 ms, causing material damage like melting, ejection of clusters and droplets, and release of hydrogen isotopes. ELM events have also long-term effects such as degradation of thermophysical properties due to cyclic heat loading (Zhitlukhin *et al.* 2007, Naujoks 2006). Experimental observations of cracks developing in tungsten subjected to transient heat loads exist in the literature, for example Pestchanyi and Linke (2007) and Garkusha *et al.* (2009). An example of such experimental observations of tungsten surface damage is shown in Fig. 1.

Recently tungsten has become a primary candidate material for Plasma-Facing Components, because it has good thermophysical properties, a high melting point, a low sputtering rate, and a low tritium inventory (Kajita *et al.* 2009). Models that describe and study the change in tungsten structure and the damage that takes place are critical in determining the limits for its operating conditions in environments with extreme heat fluxes. The main objective of this paper is to develop a computational model for thermo-mechanical damage in tungsten under transient energetic ion bombardment conditions. Recent experiments have shown that under helium and hydrogen ion bombardment conditions, some near-surface grains are observed to be ejected from the bulk to the surface region (Ohno *et al.* 2007). Simulation of tungsten damage and micro-crack formation, as well as other types of surface damage, such as swelling and grain ejection, are explained. In the next section, the main thermophysical properties of tungsten are given, followed by the theoretical background of the present model. A description of the computational model is then given in subsection 2.4. The main results are presented and discussed in section 3, and conclusions of the work are presented in section 4.

2. Theoretical background

2.1 Review of tungsten properties

Tungsten is a high-Z material that has the lowest coefficient of thermal expansion of all pure metals. White (1959) has developed an empirical equation to calculate the coefficient of thermal expansion at a given temperature

$$\alpha = 4.35 \times 10^{-6} + 0.3 \times 10^{-9}T + 0.51 \times 10^{-12}T^2 \quad (1)$$

where α ($1/^\circ\text{C}$) is the coefficient of thermal expansion and T is the temperature in $^\circ\text{C}$.

Other thermal properties for different ranges of temperature can be calculated from the following equations extracted from the ITER Material Properties Handbook (IMPH)

$$k = 174.93 - 0.11T + 5.01 \times 10^{-5}T^2 - 7.83 \times 10^{-9}T^3, \quad T = 293 \rightarrow 3773(\text{K}) \quad (2)$$

$$c_p = 128.31 + 3.28 \times 10^{-2}T - 3.41 \times 10^{-6}T^2, \quad T = 293 \rightarrow 3273(\text{K}) \quad (3)$$

$$\rho = 19302.7 - 0.24T - 2.24 \times 10^{-8}T^2, \quad T = 293 \rightarrow 1773(\text{K}) \quad (4)$$

where k ($\text{W}/(\text{m K})$) is the thermal conductivity, c_p ($\text{J}/(\text{kg K})$) is the specific heat at constant pressure, and ρ (kg/m^3) is the density. One of the other important properties of tungsten is its high melting point, $T_m \approx 3700$ K. Tables 1 and 2 summarize key mechanical properties, and the values of the fracture toughness for tungsten at different temperatures.

2.2 Coupled thermal and mechanical model

In Tokamak-type plasma applications, such as in JET or ITER, the divertor is subjected to transient high heat loads that propagate inside the divertor material by heat conduction. This is described with the heat equation that takes the general form

$$\rho c_p \frac{\partial T}{\partial t} + \nabla \cdot (-k \nabla T) = Q - \rho c_p \mathbf{u} \cdot \nabla T \quad (5)$$

where Q is a heat source, and k is the thermal conductivity. In the absence of a convective flow, the velocity, \mathbf{u} , can be set to zero to get the pure conductive heat equation

$$\rho c_p \frac{\partial T}{\partial t} + \nabla \cdot (-k \nabla T) = Q \quad (6)$$

To simulate transient conditions of the plasma, the tungsten surface is subjected to a heat flux from one side, on the form of

$$-\mathbf{n} \cdot \mathbf{q} = q_o + h(T_\infty - T) \quad (7)$$

Where \mathbf{n} is the normal vector to the surface, T_∞ is the material reference temperature, h is the heat transfer coefficient, q_o is the inward heat flux normal to the boundary, and \mathbf{q} is the total heat flux vector

$$\mathbf{q} = -k \nabla T + \rho c_p \mathbf{u} T \quad (8)$$

In order to perform thermo-mechanical analysis, a boundary value problem (BVP) is formulated for an elastic material response with the properties listed in Table 1. The BVP is constructed by substituting the constitutive equation for linear elasticity

$$\sigma_{ij} = C_{ijkl}(\varepsilon_{kl} - \varepsilon_{kl}^\theta) \quad (9)$$

Table 1 Typical mechanical properties of tungsten at different temperatures

	200 (K)	1000 (K)	2500 (K)
Young's modulus (GPa)	420	380	250
Shear modulus (GPa)	156	142	115
Poisson's ration	0.28	0.3	0.32
Tensile yield strength (MPa)	380	300	250

into the strong form of the equilibrium equation

$$\sigma_{ij,j} + f_i = 0 \quad (10)$$

where σ (Pa) is the symmetric stress tensor, \mathbf{f} (N/m³) is body force, ε is the total strain tensor, and ε^θ is the strain tensor due to thermal expansion defined respectively as

$$\varepsilon_{ij} = \frac{1}{2}(u_{i,j} + u_{j,i}), \quad \varepsilon_{ij}^\theta = \alpha\theta\delta_{ij} \quad (11)$$

where θ is the temperature increase and \mathbf{C} is the stiffness tensor.

The result of this substitution is Navier's equation

$$(\lambda + \mu)u_{j,ji} + \mu u_{i,jj} + f_i - (3\lambda + 2\mu)\alpha\theta_{,i} = 0 \quad (12)$$

where μ and λ are Lamé constants, along with the boundary conditions

$$\begin{cases} \sigma_{ij}n_j = t_i \text{ on } \partial\beta_t \\ u_i = \bar{u}_i \text{ on } \partial\beta_u \end{cases} \quad s.t. \quad \partial\beta_u \cup \partial\beta_t = \beta \quad \partial\beta_u \cap \partial\beta_t = \emptyset \quad (13)$$

where $\partial\beta_u$ and $\partial\beta_t$ are parts of the total boundary, β , where prescribed displacement, \bar{u}_i , and prescribed traction, t_i , are applied respectively.

A damage mechanics model is included for grain boundary sliding and decohesion, utilizing contact mechanics. The penalty method, in which an algorithm is set up to solve a constrained optimization problem, is constructed as

$$f_\varepsilon(\mathbf{x}) = f(\mathbf{x}) + \frac{1}{2\varepsilon}[g(\mathbf{x})]^2 \quad (14)$$

where $f_\varepsilon(\mathbf{x})$ is the penalty function, $f(\mathbf{x})$ is the original function subjected to optimization, $g(\mathbf{x})$ is a gap function defined between the master and slave boundaries, and ε is a penalty factor. The original constrained problem is replaced with another un-constrained problem, where a solution can be found by finding a stationary point \mathbf{x}_ε by minimizing the above function

$$\nabla f_\varepsilon(\mathbf{x}_\varepsilon) = \nabla f(\mathbf{x}_\varepsilon) + \frac{1}{\varepsilon}g(\mathbf{x}_\varepsilon)\nabla g(\mathbf{x}_\varepsilon) = \mathbf{0} \quad (15)$$

The solution of the minimization problem will converge to the solution of the original problem as the penalty factor approaches zero, i.e. taking the limit as ε goes to zero

$$\mathbf{x} = \lim_{\varepsilon \rightarrow 0} \mathbf{x}_\varepsilon \quad (16)$$

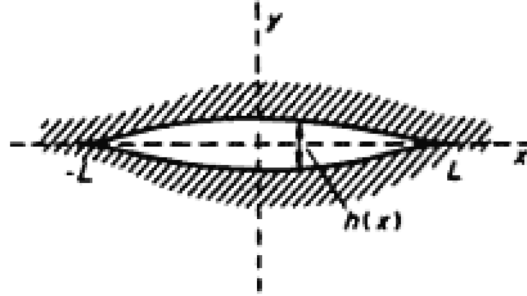


Fig. 2 Schematic representation of a crack with forces lateral to its surface (Landau and Lifshitz 1965)

2.3 Damage crack formation model

Grain boundary sliding and motion result in stress concentrations along grain boundaries, which are generally weak regions in the material susceptible to crack initiation and propagation. We consider here a crack equilibrium model to describe crack damage formation along weak grain boundaries. Consider a crack in an elastically isotropic medium, as in Fig. 2. The crack opening, $h(x)$, is given by

$$h(x) = \int_x^L \rho(\xi) d\xi \quad (17)$$

where $\rho(x)$ is interpreted as the density of straight dislocations lying along the z-direction (Landau and Lifshitz 1965), and the integral is carried over L which is half of the total crack length $2L$. Since the crack can be treated as a distribution of dislocations, the stress field generated by the crack is given by

$$\sigma_{yy} = -\frac{\mu}{2\pi(1-\nu)} \int_{-L}^L \frac{\rho(\xi) d\xi}{\xi-x} \quad (18)$$

where μ and ν are the shear modulus and poisson's ratio, respectively.

The boundary condition on the free surface of the crack requires that

$$\sigma_{yy} + p(x) = 0 \quad (19)$$

where $p(x)$ is the external load. Assuming that the edges of the crack joint smoothly near its ends, then it's necessary to take into account the forces of molecular attraction between the surfaces. If we denote the force of molecular cohesion per unit area of the crack by G , then by taking it into account, the boundary condition now becomes

$$\sigma_{yy} + p(x) = G \quad (20)$$

Inserting the expression for the crack stress field in the previous equation, and after some manipulation, we obtain

$$\int_L^0 \frac{p(x) dx}{\sqrt{L^2-x^2}} = \frac{1}{\sqrt{2L}} \int_0^d \frac{G(\xi) d\xi}{\sqrt{\xi}}, \quad d \approx L-x \quad (21)$$

This last integral depends on the material properties, and can be expressed as (Landau and Lifshitz 1965)

$$\int_0^l \frac{G(\xi) d\xi}{\sqrt{\xi}} = \sqrt{\frac{\pi \mu E}{1 - \nu^2}} \quad (22)$$

where E is the elastic modulus. Finally replacing $p(x)$ with $F\delta(x)$ will lead to an expression for the crack length that is in equilibrium with the external force per unit area, F

$$2L = \frac{F^2(1 - \nu^2)}{\pi \mu E} \quad (23)$$

As a simple constitutive damage model, we take the grain boundary thermally-induced forces on the crack surface as simply proportional to the thermal strain at the grain boundary during the transient

$$F = \alpha E \Delta T \quad (24)$$

where ΔT is the temperature difference between an assumed relaxed and stress-free state, taken to be at room temperature, to a thermally- and mechanically- stressed state at the current temperature. This last expression can be viewed in light of Eq. (11), as a thermal stress or a thermal force per unit area, and it is applied on the grain boundaries. The thermal force exhibits spatial and time dependence, as a result of the spatial dependence and time dependence of the temperature field and the locality of grain boundaries.

For macroscopic simulations, the onset of brittle fracture is usually determined by the Griffith criterion (Philip 2009), which is based on comparing the stress intensity factor to the fracture toughness. Crack initiation takes place when the stress intensity factor reaches a value greater than the material fracture toughness, i.e.

$$K \geq K_c \quad (25)$$

and

$$K = \sigma \sqrt{\pi a} \quad (26)$$

where K_c is the critical value of the material fracture toughness, and a is the crack length. The fracture toughness represents the resistance of the material to brittle crack formation (Kim 2011). Typical values for tungsten at different temperatures are presented in Table 2. The simple damage model adopted in this study is motivated by the Griffith brittle fracture criterion.

2.4 Computational model

A multiphysics computational model has been developed within a finite element framework in order to investigate the synergistic effects of transient high heat loads and helium ion irradiation. The implementation of the model utilizes the capabilities of the COMSOL commercial software multiphysics platform, in which a transient heat conduction analysis, coupled with a quasi-transient elastic structural mechanics analysis with contact elements along the grain boundaries, were solved in a segregated fashion. The simulated model is a 10 mm \times 10 mm, two-dimensional block, which was divided into a random distribution of grains. An algorithm based on the Voronoi Diagram was developed to generate a random distribution of grains as shown in Fig. 3. The grain boundaries

Table 2 Tungsten fracture toughness values for a range of temperature (Babak 1982)

T (K)	293	473	673	773	873	1073	1273	1873	2273
K (MN/m ^{3/2})	27.5	31	34.5	40	50	46	28	15	6.5

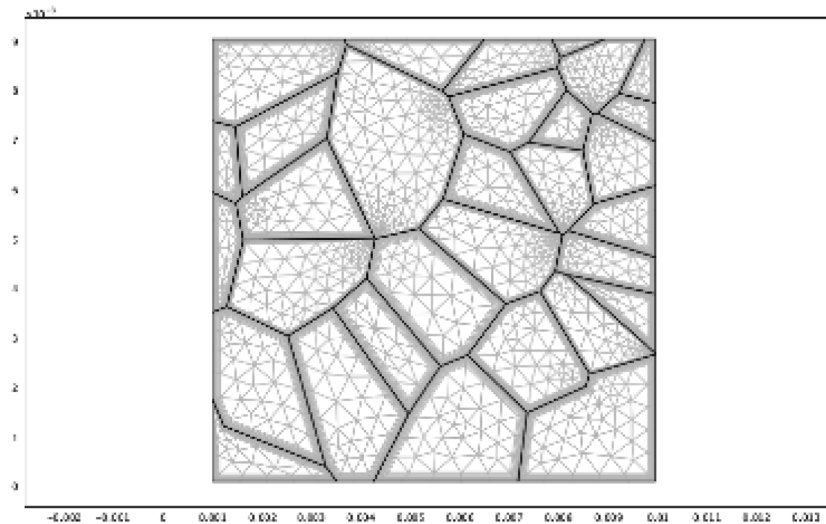


Fig. 3 Initial configuration of the random distribution of grains with boundary layer mesh, the left edge is subjected to a heat flux and is free to deform, while the right edge has convection boundary condition and is fixed. The upper and lower edges are subjected to periodic boundary conditions. The axes are the x and y coordinates

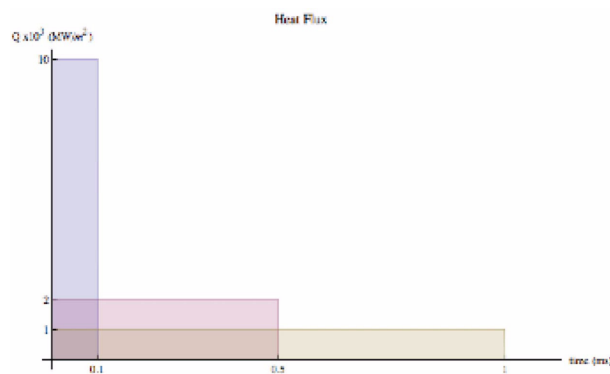


Fig. 4 Inward heat flux profile: values of the heat flux (MW/m²) vs. duration of application (ms) for the three cases considered in this study

were replaced with cohesive contact elements to better simulate sliding and opening between the grains, as a result of *He* bubble formation along grain boundaries causing the grains to open up and form micro-cracks. A boundary layer mesh was utilized along the grain boundaries, as can be seen in the figure.

Thermal boundary conditions were prescribed as an inward heat flux value, q_o , on the left side. The heat flux pulses were taken to be 10×10^3 , 2×10^3 , 1×10^3 (MW/m²), for the duration of 0.1, 0.5 and 1 ms, respectively, as shown schematically in Fig. 4. These heat flux profiles are similar to conditions expected in the ITER design during ELM transient heat loads. A convective heat flux boundary condition was applied on the other side of the tungsten plate, representing helium cooling. The mechanical boundary conditions were taken as a free surface on the left side, while the right side was fixed. Periodic boundary conditions for both the displacement and the temperature fields were used on the top and bottom boundaries of the model. The simulation duration was taken as 0.1 s, with time steps of 0.1 ms using a segregated solver that combines transient thermal analysis with the quasi-static mechanical analysis.

3. Results and discussion

The high heat flux applied to the surface of tungsten results in rapid thermal transients, which cause thermal expansion and contraction during the thermal transient. This, in turn, forces the grains to slide relative to each other. The relative motion between grains leads to decohesion and grain boundary separation, forming inter-granular micro-cracks. Cracks then propagate inside the material forming a networks of cracks of various spatial resolutions, which can be categorized into primary (relatively larger cracks), and secondary (relatively smaller) cracks.

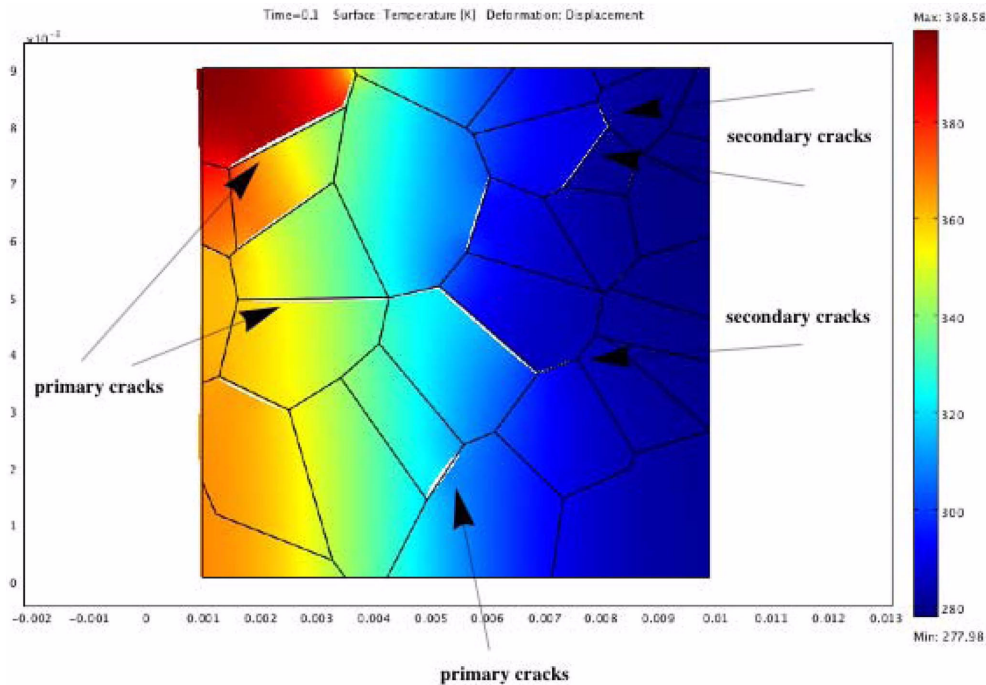


Fig. 5 Temperature distribution in [K], and tungsten grain boundary damage due to differential thermal expansion/contraction and crack formation when subjected to $Q = 1 \times 10^3$ (MW/m²). The axes are the x and y coordinates of the model

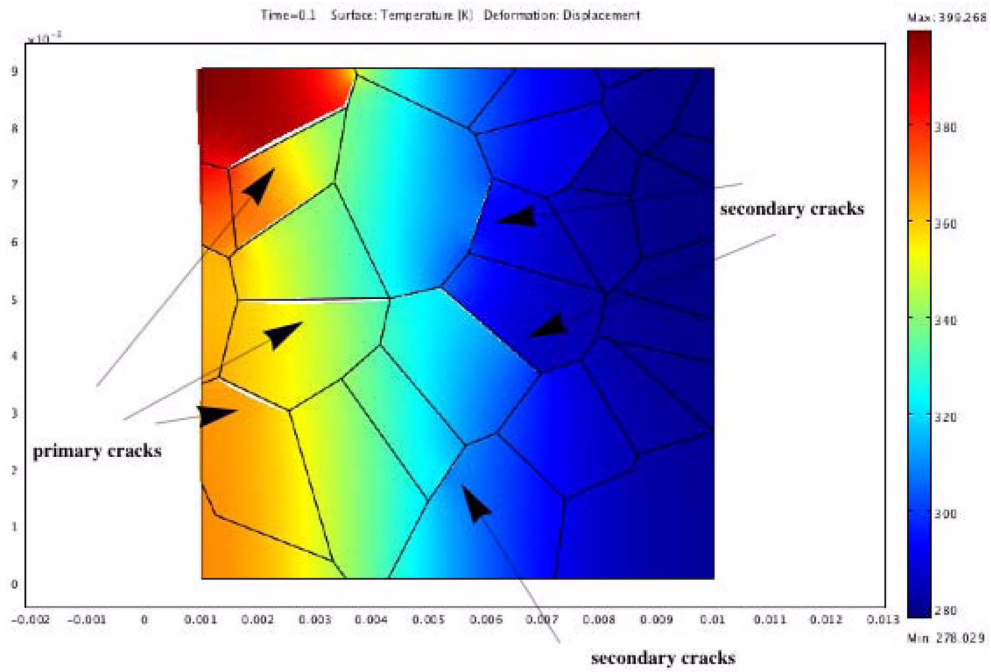


Fig. 6 Temperature distribution in [K] and tungsten damage due to differential thermal expansion/contraction and crack formation when subjected to $Q = 2 \times 10^3$ (MW/m²). The axes are the x and y coordinates of the model

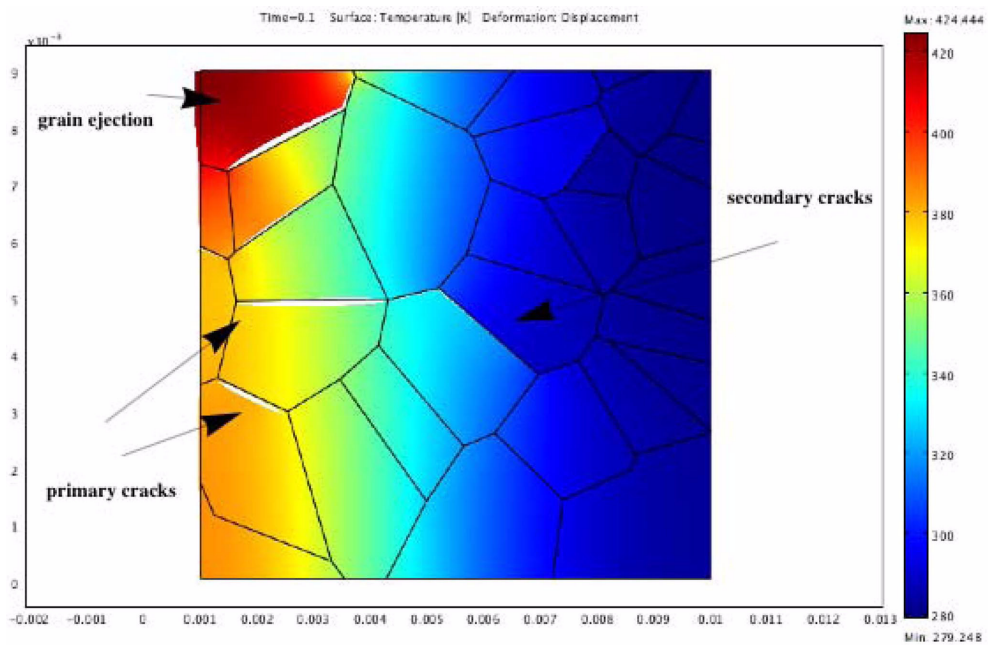


Fig. 7 Temperature distribution in [K] and tungsten damage due to differential thermal expansion/contraction and crack formation when subjected to $Q = 1 \times 10^4$ (MW/m²). Grain ejection also happened under this condition of heat flux. The axes are the x and y coordinates of the model

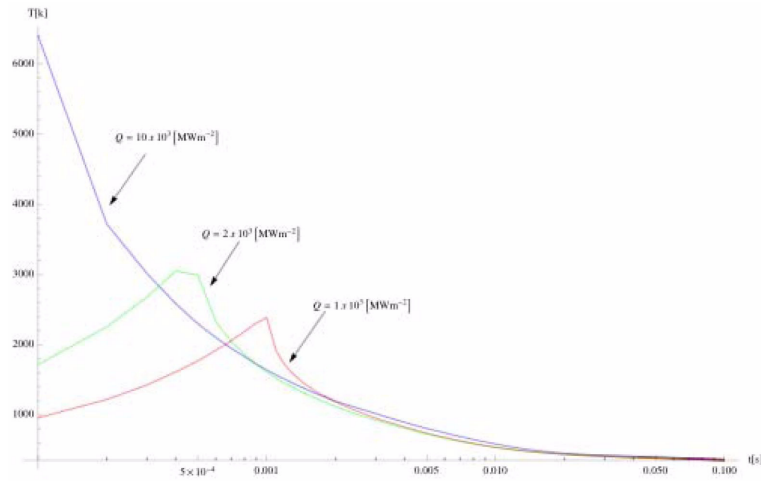


Fig. 8 Transient temperature profiles of a point on the tungsten surface, plotted on a semi-log scale for the three different values of Q

Typical results at the end of the simulation that show the onset of cracks of different sizes are shown in Figs. 5, 6, and 7. It is noted that the temperature rises to very high values exceeding the melting point for the case when the heat flux was 1×10^4 (MW/m^2). Our model does not directly address the ensuing evaporation of tungsten from the surface in such severe conditions, as experimentally observed, for example in references (Garkusha *et al.* 2005) and (Bazylev *et al.* 2005). The temperatures of the surface at the end of the different simulations are shown in Fig. 8.

We note the difference in the distribution and in the size of cracks for the different applied heat fluxes. We see from the results that the cracks have larger sizes for the case when the heat flux was 1×10^4 (MW/m^2), but they are more close to the surface. While for the case when the heat flux was 1×10^3 (MW/m^2), the cracks are smaller in size, and are formed at deeper distances from the surface of tungsten. This is due to the difference in heat propagation for the different heat flux profiles.

Another aspect of tungsten surface damage is grain ejection from the bulk onto the surface during transients, which has been experimentally observed in tungsten subjected to *He* irradiation (Ohno *et al.* 2007). When the tungsten surface is subjected to *He* and D^+ bombardment at high temperature, helium and vacancies diffuse to grain boundaries forming grain boundary bubbles. When the surface is subsequently subjected to a transient heat load, *He* bubbles grow and expand rapidly along grain boundaries, causing substantial pressure on grain faces. When the pressure exceeds a critical value that is greater than the cohesive forces on grain boundaries, grains may completely separate resulting in the phenomenon of grain ejection.

4. Conclusions

The effects of transient plasma heat loads, such as edge localized modes (ELMs), on tungsten thermal and mechanical properties, were successfully studied through the development of a multiphysics model that combines mechanical and thermal transient analysis. When the surface of

tungsten is subjected to plasma ion bombardment, it generates high heat fluxes that cause substantial increase in the temperature of the tungsten surface. The multiphysics thermo-mechanical model indicates that transient heating of tungsten that is already containing helium bubbles, will result in the evolution of sub-surface residual stresses, material swelling, grain boundary sliding, and sub-surface mechanical damage. As a consequence, degradation of tungsten thermophysical properties will result from such rapid thermal transients. Primary and secondary inter-granular micro-cracks are a manifestation of surface damage, and it was observed that their size and depth from the surface vary with the heat load profile. Another simulated type of mechanical damage was grain ejection, which results from the complete separation between grains that are close to the surface.

References

- Babak, A.V. (1982), "Evaluating the crack resistance of tungsten at high temperatures", *Strength Mater.*, **14**(10), 1389-1391.
- Bazylev, B.N., Janeschitz, G., Landman, I.S. and Pestchanyi, S.E. (2005), "Erosion of tungsten armor after multiple intense transient events in ITER", *J. Nucl. Mater.*, **337-339**, 766-770.
- Garkusha, I.E., Bandura, A.N., Byrka, O.V., Chebotarev, V.V., Landman, I., Makhraj, V.A., Pestchanyi, S. and Tereshin, V.I. (2009), "Damage to preheated tungsten targets after multiple plasma impacts simulating ITER ELMs", *J. Nucl. Mater.*, **386**, 127-131.
- Garkusha, I.E., Bandura, A.N., Byrka, O.V., Chebotarev, V.V., Landman, I.S., Makhraj, V.A., Marchenko, A.K., Solyakov, D.G., Tereshin, V.I., Trubchaninov, S.A. and Tsarenko, A.V. (2005), "Tungsten erosion under plasma heat loads typical for ITER type-I LEMs and disruptions", *J. Nucl. Mater.*, **337-339**, 707-711.
- Iwakiri, H., Yasunaga, K., Morishita, K. and Yoshida, N. (2000), "Microstructure evolution in tungsten during low-energy helium ion irradiation", *J. Nucl. Mater.*, **283**, 1134-1138.
- Kajita, S., Ohno, N., Sakaguchi, W. and Takagi, M. (2009), "Visualized blow-off from helium irradiated tungsten in response to ELM-like heat load", *Plasma Fusion Res.*, **4**, 4.
- Kim, C.I. (2011), "An analysis of an elastic solid incorporating a crack under the influences of surface effects in plane and anti-plane deformations", *Interact. Multiscale Mech.*, **4**(2), 123-137.
- Landau, L.D. and Lifshitz, E.M. (1965), *The theory of elasticity*, Nauka, Moscow.
- Naujoks, D. (2006), *Plasma-material interaction in controlled fusion*, Springer.
- Ohno, N., Kajita, S., Dai, Nishijima, and Takamura, S. (2007), "Surface modification at tungsten and tungsten coated graphite due to low energy and high fluence plasma and laser pulse irradiation", *J. Nucl. Mater.*, **363**, 1153-1159.
- Pestchanyi, S.E. and Linke, J. (2007), "Simulation of cracks in tungsten under ITER specific transient heat loads", *Fusion Eng. Des.*, **82**(15-24), 1657-1663.
- Philip, P. (2009), "A quasistatic crack propagation model allowing for cohesive forces and crack reversibility", *Interact. Multiscale Mech.*, **2**(1), 31-44.
- Tokunaga, K. (2003), "Surface morphology and helium retention on tungsten exposed to low energy and high flux helium plasma", *J. Nucl. Mater.*, **313-316**, 92-96.
- Tokunaga, K., Yoshikawa, O., Makise, K. and Yoshida, N. (2002), "Effects of helium irradiation on high heat load properties of tungsten", *J. Nucl. Mater.*, **307**, 130-134.
- White, J.L. (1959), *Physicochemical measurements at high temperatures*, Ed. J O'M Bockris J L White and J D Mackenzie, London, Butterworths.
- Xu, Q., Yoshida, N. and Yoshiie, T. (2007), "Accumulation of helium in tungsten irradiated by helium and neutrons", *J. Nucl. Mater.*, **367-370**, 806-811.
- Zhitlukhin, A., Klimov, N., Landman, I., Linke, J., Loarte, A., Merola, M., Podkovyrov, V., Federici, G., Bazylev, B., Pestchanyi, S., Safronov, V., Hirai, T., Maynashev, V., Levashov, V. and Muzichenko, A. (2007), "Effects of ELMs on ITER divertor armour materials", *J. Nucl. Mater.*, **363-365**, 301-307.